

## ***N*-[Salicylidene-1,2-ethanediaminoethyl]-2-bromoisobutyramide as initiator for atom transfer radical polymerization and surface-initiated ATRP of methyl methacrylate on copper**

Gang Lu · Yi-Min Li · Chun-Hua Lu · Zhong-Zi Xu

Received: 4 January 2010 / Revised: 17 February 2010 / Accepted: 4 March 2010 /  
Published online: 13 March 2010  
© Springer-Verlag 2010

**Abstract** *N*-[Salicylidene-1,2-ethanediaminoethyl]-2-bromoisobutyramide (SEB) was synthesized and characterized by elemental analysis, FT-IR and <sup>1</sup>H NMR. It had been successfully used as a bidentate initiator for the atom transfer radical polymerization (ATRP) of methyl methacrylate with CuBr/2,2'-bipyridine as the catalyst and *N,N*-dimethylformamide as the solvent at 70 °C. The kinetics was first order in monomer and the number-average molecular weight of the polymer increased linearly with monomer conversion, indicating the 'living'/controlled nature of the polymerization. The polymerization reached high conversions producing polymers with a low molecular weight distribution ( $M_w/M_n = 1.34$ ). The obtained poly(methylmethacrylate) (PMMA) functionalized with salicylidene-1,2-ethanediaminoethyl and  $\omega$ -Br as the end groups were characterized by FT-IR spectroscopy. They can be used as macroinitiators for chain-extension reaction. Then, PMMA coatings were grafted from copper substrates by surface-initiated ATRP from a surface-bound SEB initiator. The electrochemical impedance spectroscopy measurements and potentiodynamic electrochemical experiments confirmed the successful grafting of the polymer coatings. Greatly improved short-term anticorrosive properties for PMMA modified electrodes were demonstrated by substantially increased resistance of the film for a period of 24 h as compared to bare copper.

**Keywords** Atom transfer radical polymerization · Electrochemical impedance spectroscopy · Potentiodynamic polarization · *N*-Salicylidene-diethylenetriamine · PMMA-covered copper electrodes · Surface-initiated ATRP

---

G. Lu (✉) · Y.-M. Li · C.-H. Lu · Z.-Z. Xu  
School of Material Science and Engineering, Nanjing University of Technology, Nanjing 210009,  
People's Republic of China  
e-mail: lugang3314@163.com

## Introduction

One of the most successful polymerization methods in the field of controlled/‘living’ radical polymerization is atom transfer radical polymerization (ATRP). It is based on the reversible dynamic equilibrium between the active and the dormant species catalyzed by a transition metal complex. ATRP allows the preparation of a wide range of polymeric materials with controlled molecular weights and well-defined architectures [1–7]. As its wide uses, intensive investigation has been conducted and large effort has been directed toward the role and the selection criteria of each component of the polymerization mixture (monomer, initiator, transition metal, and ligand) [8, 9].

The initiator is very important because it has to form an initiating radical species via homolytic cleavage of its labile bond such as C–halogen by the catalyst. In early stages, the initiators employed in ATRP were mainly alkyl halides. In 1995, an alkyl chloride (1-phenylethyl chloride, 1-PECl) and carbon tetrachloride ( $\text{CCl}_4$ ) were almost simultaneously reported by Matyjaszewski and Xia [1] and Sawamoto et al. [10, 11]. Afterwards, other organic halides, such as halo ketones, halo esters, halo amides, halonitriles, and sulfonyl halides were successfully employed in conventional ATRP [1, 11].

So far, in the area of ATRP, most of the initiators successfully studied are organic halides with a potentially active carbon–halogen bond because fast initiation is vital to obtain well-defined polymers with narrow polydispersities [1]. However, high stabilization of the initiating radical may cause slow initiation, and slow initiation may cause uncontrolled polymerization and high polydispersities polymers, thus, some halogens ( $\text{R-X}$ ,  $\text{X} = \text{I}$ ) are not powerful according to the results reported [1, 11]. The other aspect of the initiators is that the initiators used determine the molecular weight of the obtained polymers and its end groups. So the initiator should be selected carefully according to its structure and the catalyst.

In the past few years, imidazole-containing polymers have been widely prepared by living ionic polymerization, due to their attractive chemical properties and their potential use as basic compounds for electrically conducting materials (e.g., solid electrolytes) [12–15]. However, living ionic polymerization requires very strict reaction conditions, which makes it difficult to be performed, and the choice of monomers is quite limited. As discussed above, ATRP not only can provide polymers with controlled molecular weights and narrow polydispersities, but also can be performed using ordinary radical polymerization procedures for various monomers, avoiding the strict conditions needed for living ionic polymerization [1, 16]. Furthermore, functional polymers with low polydispersities and specific end groups can be obtained by using functional initiators in ATRP [17].

An important application of ATRP is the grafting of polymer brushes from the surfaces of flat substrates and colloidal particles. Specially designed surface-attachable ATRP initiators can be immobilized onto the surface, followed by in situ ATRP. An important advantage of this “grafting from” [18–22] method compared to other polymerization grafting methods is the ability to produce polymer brushes with high grafting density.

By grafting polymers with different functionalities, the modified metals become feasible for applications in different areas. For example, by grafting PEG-type [23] or phosphorylcholine-type [24] polymers, the nonspecific protein adsorptions on metal surfaces can be well prohibited, which is extremely useful for improving the biocompatibility of metal-made bioimplants. Fluoropolymers have a lot of interesting properties, such as high thermal, chemical, and photochemical stability; low refractive index; and low surface energy. The grafting of fluoropolymers makes metal surfaces become “self-cleaning” due to the polymer’s excellent water- and oil-repellent properties [25]. The high stability of fluoropolymers in all environments can also provide excellent protections to metals from chemical corrosions and photodegradations.

Although there are many different materials that have been successfully used as substrates for surface-initiated ATRP (SI-ATRP) [26–29], some of the most common and important materials in our everyday life, iron, copper, and alloys, have been largely overlooked by researchers. Unlike other kinds of materials, the surfaces of metals have chemical and physical properties that make them attractive materials for manufacturing. The ability of copper to inhibit the growth of bacteria, viruses, and fungi motivates its use in the fabrication of water pipes and doorknobs. Both metals have excellent electrical and thermal conductivities. As the most efficient conductor of electricity and heat among nonprecious metals, copper, and iron might be the most extensively used material in electric and electronic devices. Both iron and copper are important components of many important alloys. Despite of all these important applications of iron and copper, no work has been reported on direct grafting of polymers from these two metals.

Therefore, in our work, a new functional initiator *N*-[salicylidene-1,2-ethanediaminoethyl]-2-bromoisobutyramide (SEB) was synthesized, and the properties of ATRP of methyl methacrylate (MMA) with this new initiator were investigated under the different conditions. Then, poly(methylmethacrylate) (PMMA) coatings were grafted from copper substrates by SI-ATRP from a surface-bound SEB initiator. The anticorrosive capabilities for the PMMA modified electrodes were studied by electrochemical impedance spectroscopy (EIS) in NaCl solutions.

## Experiment part

### Materials

MMA (Chemically Pure, Sinopharm Chemical Reagent Co. Ltd.) and triethylamine (Chemically Pure, Shanghai Kaidi Chemical Reagent Co. Ltd.) were purified by vacuum distillation. 2,2'-Bipyridine (bpy) (Analytical Reagent, Shanghai Lingfeng Chemical Reagent Co. Ltd.), tetrahydrofuran (THF) (Analytical Reagent, Shanghai Yishi Chemical Reagent Co. Ltd.), methanol (Analytical Reagent, Sinopharm Chemical Reagent Co. Ltd.), 2-bromoisobutyryl bromide (BiBB) (98%, Acros Organics), *N,N*-dimethylformamide (DMF) (Analytical Reagent, Sinopharm Chemical Reagent Co. Ltd.), copper(I) bromide (CuBr) (98%, Acros Organics), methylbenzene (Analytical Reagent, Shanghai Kaidi Chemical Reagent Co. Ltd.),

diethylenetriamine (DETA) (Analytical Reagent, Sinopharm Chemical Reagent Co. Ltd.) were used as purchased. *N*-Salicylidene-diethylenetriamine and distilled water was self-made.

### Synthesis of SEB

In a 200-mL flask equipped with a reflux condenser and a dropping funnel, there were placed 11 g of DETA and 12 mL of methylbenzene, and the reaction mixture was kept at 115 °C with magnetically stirring. 12 g of salicylaldehyde and 23 mL of methylbenzene were dropped during 60 min to the solution through the dropping funnel, which was stirred for 1.5 h at 115 °C. Then the resulting solution was purified by vacuum distillation, the product was *N*-salicylidene-diethylenetriamine. Then, a 100 mL of flask with a magnetic stirrer was purged with nitrogen for 10 min. *N*-Salicylidene-diethylenetriamine (3 g), triethylamine (3 mL), and methylbenzene (10 mL) were added after the flask was cooled to 0 °C using ice/water bath. Then the solution of BiBB (1.972 mL, 8 mL methylbenzene) was added slowly in 2 h via a syringe and a yellow precipitate formed immediately. After BiBB was added completely, the reaction persisted 24 h at 0 °C. The reaction mixture was extracted with distilled water to remove the amine salt. At last, the solvent methylbenzene and residual triethylamine were removed under vacuum, the final product was SEB.

### Polymerization of MMA via ATRP

The general procedure of the polymerization was as follows: CuBr (0.068 g), bpy (0.1473 g), MMA (10 mL), and *N,N*-dimethylformamide (10 mL, 50% v/v) were added to an ampule tube under stirring, three cycles of vacuum nitrogen were applied in order to remove the oxygen. After the catalyst was dissolved (about 10 min), SEB (0.1678 g) was added via syringe. Then the ampule tube was sealed under nitrogen and placed in a water bath thermostated at the desired temperature. Aliquots were taken and placed into an ice bath to stop the reaction periodically via syringes to follow the kinetic of the polymerization process. The aliquots were diluted with THF followed by filtration through a basic alumina column prior to PMMA isolated by precipitation in methanol and dried in vacuum at 25 °C for 24 h.

### SI-ATRP of MMA on copper coupons

The 1 cm thick copper coupons were polished sequentially up to 1,200 grit SiC paper. The newly polished coupons were washed with copious amounts of deionized water, acetone, ethanol, and deionized water, in that order, for 5 min each to degrease and clean the surface. Then, freshly cleaned copper coupons were immersed in a 2.5 mg/mL DMF solution of SEB for 12 h at room temperature for self-assembly. The modified coupons were rinsed with copious amount of deionized water to remove unattached initiator and dried under a stream of dry N<sub>2</sub>. For the preparation of PMMA brushes on the copper surface, MMA (10 mL), CuBr (0.068 g), and bpy (0.1473 g) was added together, and then the copper coupons were introduced into the reaction mixture under N<sub>2</sub> protection. The reaction tube

was sealed and kept in 70 °C water bath to produce copper-PMMA surfaces. After 1, 3, and 5 h, the coupons were removed from the reaction tube and were quickly rinsed with deionized water and dried under N<sub>2</sub>.

### Characterization

Conversion of monomer was determined by gravimetry. Number-average molecular weights and molecular weight distributions of polymers obtained were measured using a Waters 515 GPC, equipped with microstyragel column (HR1, HR3, and HR4) with THF as a mobile phase at a flow rate of 1 cm<sup>3</sup>/min operated at 25 °C. Linear polystyrene standards were used for calibration. <sup>1</sup>H NMR spectra was recorded in deuterated chloroform (CDCl<sub>3</sub>) using tetramethylsilane (TMS) as internal reference on a Bruker AV400 spectrometer at ambient temperature. FT-IR spectra was using MAGNA-IR 750 (Nicolet Instrument Co. USA) model FT-IR spectrometer in the 4000–400 cm<sup>-1</sup> region by dispersing the sample in KBr Discs. The complex was characterized by the elemental analyses using Vario El-III CHNSO elemental analyzer (Elementar Co., Germany).

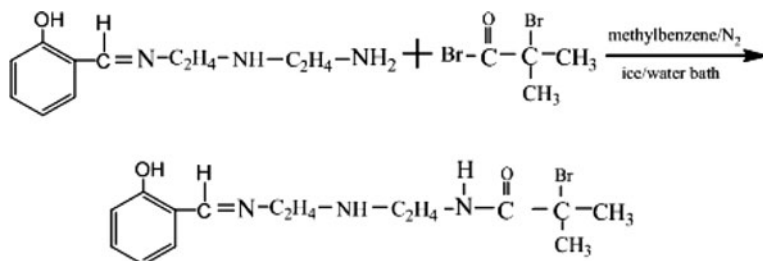
### Electrochemical measurements

To assess the anticorrosion properties of the surface-functionalized coupons of copper (self-assembled SEB monolayers and copper-PMMA), impedance spectra was used. The pristine and the surface-functionalized coupons were mounted in a PVDF holder, leaving a circular area of 1 cm<sup>2</sup>, to serve as the working electrode. The cell for electrochemical measurements was a traditional three-electrode cell. The working electrode was copper electrode, a platinum wire was used as a counter electrode, and the reference electrode was a saturated calomel electrode (SCE). The working electrode was facing downward while the counter electrodes were placed vertically facing each other. The reference electrode was led to the surface of the working electrode through a Luggin capillary. The impedance measurements were performed 0.5 h after the electrode had been immersed in the electrolyte. The electrochemical measurements were performed with IM6 electrochemical workstation (ZAHNER, Germany). Impedance measurements were performed under free corrosion potential ( $E_{\text{corr}}$ ) with a sinusoidal potential perturbation of 10 mV in amplitude and frequency from 100 kHz to 10 MHz. The data of impedance spectra were fitted to probable equivalent circuits (ECs) using the program ZVIEW (version 3.0, Scribner Associates, Inc.). Potentials reported in our paper were all referred to SCE and the solution was 0.5 mol/L NaCl solution.

## Results and discussion

### Synthesis and characterization of the new initiator

SEB as shown in Scheme 1 could be easily obtained. SEB was a kind of *N*-heterocyclic compound containing alkyl bromide group, so it can be used for



**Scheme 1** Synthesis of the new initiator

ATRP as initiator. The new initiator was checked using elemental analysis, FT-IR spectra and  $^1\text{H}$  NMR spectra.

Analytical results of the composition of SEB of carbon, hydrogen, and nitrogen were given in Table 1. The results agreed well with the calculated value and were consistent with the proposed structure.

In the  $^1\text{H}$  NMR spectrum of the initiator (Fig. 1), all the signals corresponding to the proposed structure were observed in  $\text{CDCl}_3$ . The hydroxyl protons (A) was assigned at  $\delta = 10.00$  ppm. The protons of benzene ring (B) were observed at  $\delta = 6.86$  ppm. The proton (C) appeared at  $\delta = 8.35$  ppm. The methylene protons (D) were observed at  $\delta = 2.80$ – $3.10$  ppm. The proton of acidamide (E) was

**Table 1** Elemental analysis results of SEB

|            | % N   | % C   | % H  |
|------------|-------|-------|------|
| Found      | 12.05 | 51.20 | 6.66 |
| Calculated | 11.80 | 50.56 | 6.18 |

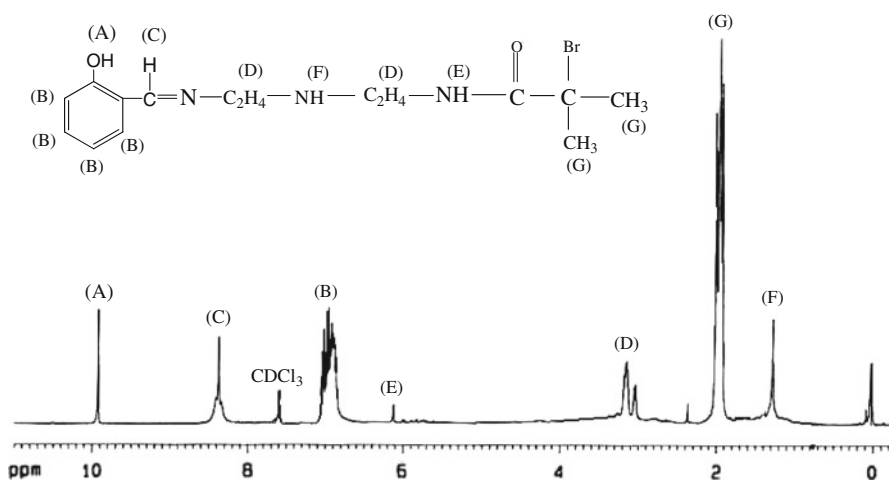


**Fig. 1**  $^1\text{H}$  NMR spectrum of the new initiator SEB in  $\text{CDCl}_3$

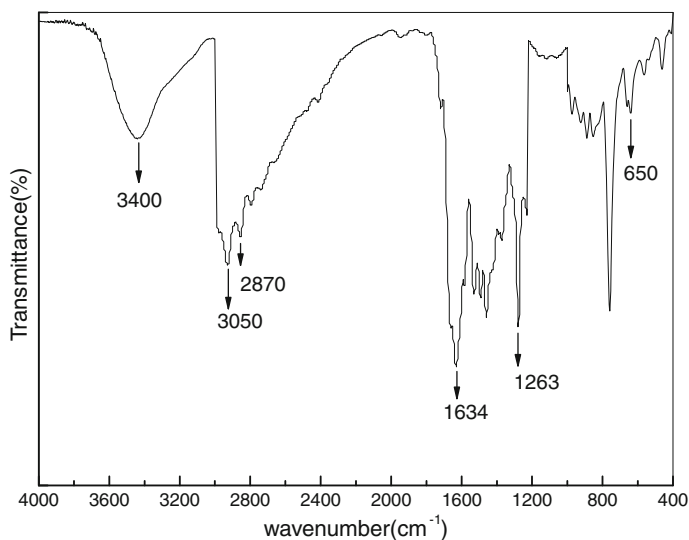


**Fig. 2** FT-IR spectrum of SEB

assigned at  $\delta = 6.10$  ppm. The peaks at  $\delta = 2.00$  ppm is ascribed to molar contributions of the methyl protons (G). The proton of secondary amine (F) appeared at  $\delta = 1.26$  ppm.

FT-IR spectra of SEB (Fig. 2) exhibited the characteristic absorptions between  $1620$  and  $1640$   $\text{cm}^{-1}$  (C=N stretching);  $3320$ – $3340$   $\text{cm}^{-1}$  (N–H stretching of secondary amine);  $3050$ – $3070$   $\text{cm}^{-1}$  (N–H stretching of acidamide);  $1260$ – $1280$   $\text{cm}^{-1}$  (C–N stretching);  $2850$ – $2870$   $\text{cm}^{-1}$  (C–H stretching of methyl);  $640$ – $650$   $\text{cm}^{-1}$  (C–Br stretching). The data above illustrated that the product was confirmed to be SEB exactly.

#### ATRP of MMA with the new initiating system

Polymerization of MMA with the condition of  $[\text{MMA}]_0:[\text{SEB}]_0:[\text{CuBr}]_0:[\text{bpy}]_0 = 200:1:1:2$  was carried out in DMF at  $70$   $^\circ\text{C}$ , the polymerization reached  $87.45\%$  within  $12$  h at  $70$   $^\circ\text{C}$  to yield PMMA of  $M_n = 23300$  and  $M_w/M_n = 1.34$ . The linear dependence of  $\ln[\text{M}]_0/[\text{M}]$  on reaction time indicated that the kinetics were first order in monomer and that the living radical concentrations were constant during the polymerization process, as observed from Fig. 3. From the same figure, it also can be seen that the monomer conversion increased with the reaction time. Figure 4 showed that the experimental molecular weights increased linearly with monomer conversion with quite narrow polydispersity index ( $1.34$ – $1.61$ ), indicating the absence or an insignificant amount of transfer reaction. However, the experimental molecular weights were higher than the calculated ones ( $M_{n,\text{th}}$ ), which were calculated as  $M_{n,\text{th}} = [\text{monomer}]_0/[\text{initiator}]_0 \times \text{conversion} \times M_{\text{monomer}} + M_{\text{initiator}}$ . The efficiencies ( $f$ ) of initiator, calculated as  $f = M_{n,\text{th}}/M_{n,\text{GPC}}$  were relatively low ( $0.18$ – $0.75$ ). This may be attributed to the back strain effect [30] and

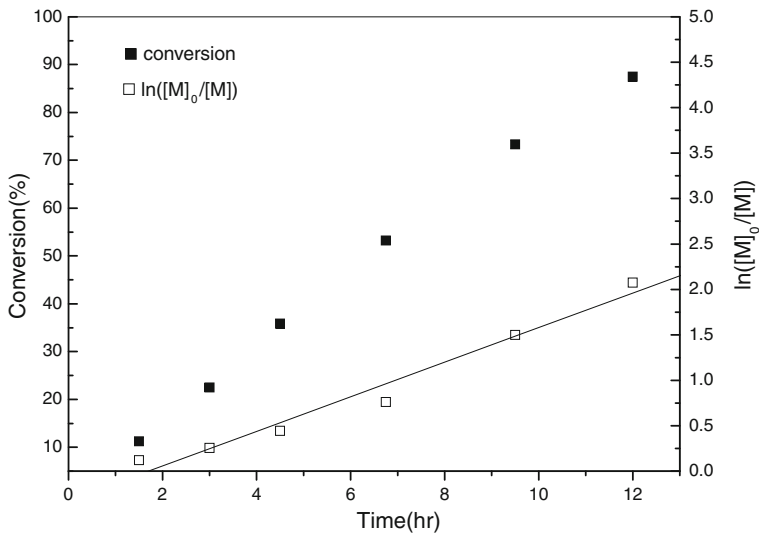


**Fig. 3** Plots of conversion and  $\ln([M]_0/[M])$  versus time for the ATRP of MMA initiated by SEB in DMF at 70 °C,  $[MMA]_0:[SEB]_0:[CuBr]_0:[bpy]_0 = 200:1:1:2$ , DMF: 50% v/v

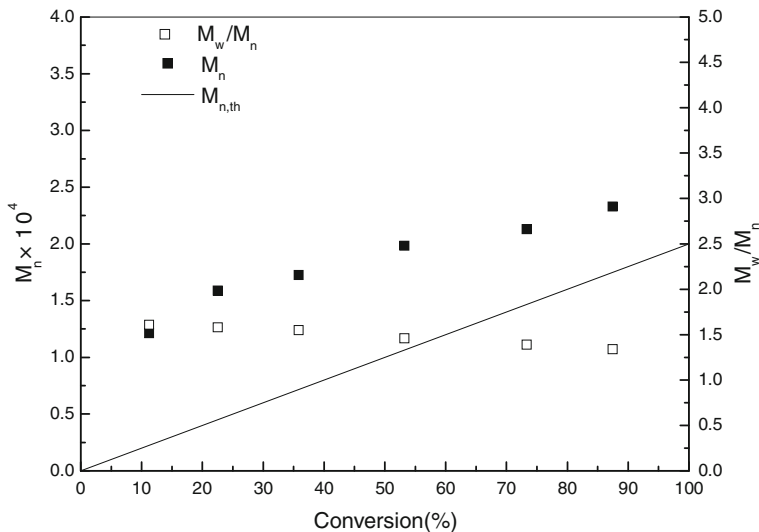


**Fig. 4** Molecular weight ( $M_n$ ) and molecular weight distribution ( $M_w/M_n$ ) dependence on monomer conversion for the polymerization of MMA under the same conditions as in Fig. 3

the steric bulky ligand. Matyjaszewski et al. [16] had reported similar results in the polymerization of MMA using EBIB/CuBr/dNBpy complex system. In their opinion, the substituent groups of the propagating radicals play a major role in the reactivity of the radicals, which should be lowered when the  $\beta$ -carbon of the radical was replaced by the substituent groups during the polymerization. This may



lead to the observed deviation from the theoretical molecular weight at lower conversion as our experiments has showed. The higher reactivity of radical with shorter chains should correlate with the lower equilibrium constant and lower overall initiator efficiency. The other explanation of the much higher  $M_{n, GPC}$  value than predicted, was the poor solubility of Cu(II) complex in the reaction systems. The propagating radicals were difficult to become dormant species by halogen transfer and underwent termination by combination reactions.

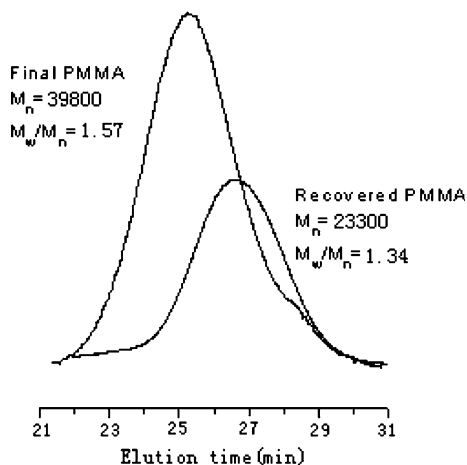
### Chain-extension reaction

If the chain end was a bromine atom, a recovered PMMA should be able to initiate the polymerization of a fresh feed of MMA in the presence of a classical ATRP system. To confirm the activity, we carried out the chain-extension polymerization of MMA using PMMA as macroinitiator ( $M_n = 23300$ ,  $M_w/M_n = 1.34$ ) prepared via ATRP with  $[MMA]_0:[SEB]_0:[CuBr]_0:[bpy]_0 = 200:1:1:2$  at 70 °C. The chain extension was conducted with fresh MMA and the component ratio  $[MMA]_0:[recovered\ PMMA]_0:[CuBr]_0:[bpy]_0 = 2000:1:10:20$  at 70 °C in DMF (50% v/v). After 12 h, the conversion reached 24.34% with  $M_n = 39800$  and  $M_w/M_n = 1.57$  (Fig. 5). The increase in the molecular weight indicated that the chain ends of the obtained macroinitiator were functionalized. However, the final PMMA had a little higher  $M_w/M_n$ , which might be due to that not all of the macroinitiator did participate in the reaction. Although most PMMA chains retained the active chain end functionality, there still some chains were “dead”.

### End group analysis

In order to gain insight into the nature of this new initiating system, the structure of the polymer  $P_{MMA-Br}$  synthesized by the SEB/CuBr/bpy system was analyzed using FT-IR spectrometer. In Fig. 6, the characteristic absorptions were obtained between 3320 and 3340  $cm^{-1}$  (N–H stretching of secondary amine); 3050–3070  $cm^{-1}$

**Fig. 5** GPC curves of polymers (recovered PMMA and final PMMA) after chain extension of PMMA synthesized by SEB/CuBr/bpy



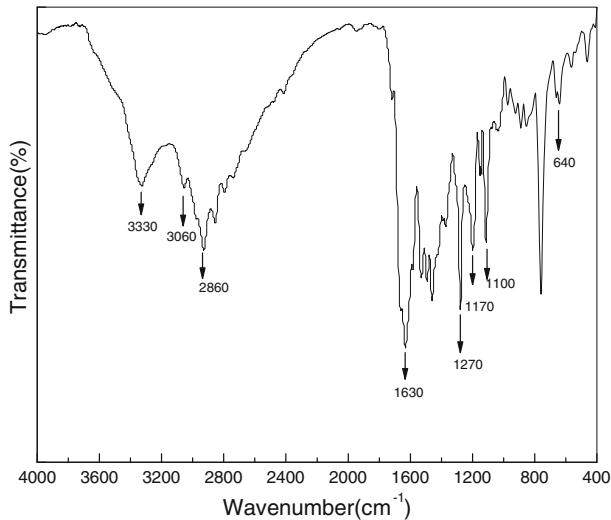


**Fig. 6** FT-IR spectrum of the  $\omega$ -Br end group of PMMA initiated with SEB/CuBr/bpy ( $[\text{MMA}]_0:[\text{SEB}]_0:[\text{CuBr}]_0:[\text{bpy}]_0 = 200:1:1:2$ ) at 70 °C. Sample:  $M_n(\text{PMMA-Br}) = 23,300$ ;  $M_w/M_n = 1.34$

(N–H stretching of acidamide); 2850–2870  $\text{cm}^{-1}$  (C–H stretching of methyl); 1620–1640  $\text{cm}^{-1}$  (C=N stretching); 1260–1280  $\text{cm}^{-1}$  (C–N stretching); 1100–1120  $\text{cm}^{-1}$  and 1150–1170  $\text{cm}^{-1}$  (C–O–C stretching of ester group); 640–650  $\text{cm}^{-1}$  (C–Br stretching). These results, including the success of chain extension with the ATRP initiating system (Fig. 5), thus confirmed that the polymer had salicylidene-1,2-ethanediaminoethyl and  $\omega$ -Br as the end groups and the polymerization should undergo an ATRP process.

#### Potentiodynamic polarization

A potentiodynamic electrochemical experiment was carried out to evaluate the corrosion resistance of PMMA-covered copper electrode in 0.5 mol/L NaCl solution, and to compare with those of SEB monolayers-covered copper and bare copper electrodes. The various electrochemical parameters, corrosion potential ( $E_{\text{corr}}$ ), corrosion current densities ( $i_{\text{corr}}$ ), Tafel slope ( $b_a$ ,  $b_c$ ), and percentage inhibition efficiencies IE (%) were calculated from potentiodynamic polarization curves and the summarized in Table 2. IE (%) was calculated as  $\text{IE}(\%) = (i_{\text{corr}}^0 - i_{\text{corr}})/i_{\text{corr}}^0 \times 100$ , where  $i_{\text{corr}}^0$  is the corrosion current densities of the bare copper electrode.

As seen in Fig. 7, the cathodic arm of the polarization curve of the SEB monolayers-covered copper electrode (curve b) was similar to that of the bare copper electrode (curve a). It was reasonable on the basis that the expected cathodic reaction should experience minimal disruption in presence of the SEB monolayers because it was under diffusion control. The anodic arm of the curve for the untreated electrode increased rapidly with increasing potential, which indicated fast metal dissolution. The form of the anodic arm of the SEB monolayers-covered copper electrode polarization curve was also characteristic of a metal ion dissolution

**Table 2** Potentiodynamic polarization parameters of copper electrodes in 0.5 mol/L NaCl solution

|                      | $E_{\text{corr}}$ versus SCE (mV) | $b_a$ (mV/dec) | $-b_c$ (mV/dec) | $i_{\text{corr}}$ ( $\mu\text{A}/\text{cm}^2$ ) | IE (%) |
|----------------------|-----------------------------------|----------------|-----------------|---|--------|
| Naked Cu             | -81                               | 60.3           | 187.4           | 26.02   | –      |
| Monolayer Cu         | -53                               | 58.7           | 182.2           | 5.23  |        |
| Cu-PMMA <sup>a</sup> | 22                                | 32.5           | 93.1            | 0.88  | 96.61  |
| Cu-PMMA <sup>b</sup> | 16                                | 44.2           | 118.1           | 0.96  | 96.21  |
| Cu-PMMA <sup>c</sup> | 11                                | 50.2           | 145.6           | 1.16  | 95.52  |

<sup>a</sup> The  $M_n$  of PMMA is  $1.27 \times 10^5$ .  $M_w/M_n$  is 1.37. The polymerization time is 11 h

<sup>b</sup> The  $M_n$  of PMMA is  $9.56 \times 10^4$ .  $M_w/M_n$  is 1.40. The polymerization time is 6 h

<sup>c</sup> The  $M_n$  of PMMA is  $7.43 \times 10^4$ .  $M_w/M_n$  is 1.59. The polymerization time is 2 h

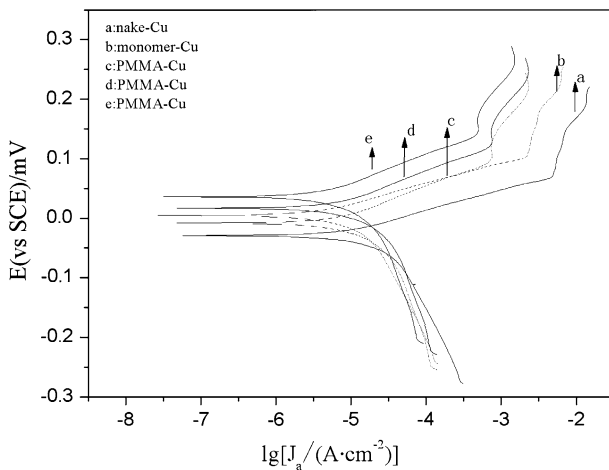


**Fig. 7** Polarization curves of copper electrodes in 0.5 mol/L NaCl solution. (a) Naked-Cu. (b) Monomer-Cu. (c) The  $M_n$  of PMMA is  $7.43 \times 10^4$ .  $M_w/M_n$  is 1.59. The polymerization time is 2 h. (d) The  $M_n$  of PMMA is  $9.56 \times 10^4$ .  $M_w/M_n$  is 1.40. The polymerization time is 6 h. (e) The  $M_n$  of PMMA is  $1.27 \times 10^5$ .  $M_w/M_n$  is 1.37. The polymerization time is 11 h

process. However, at a certain potential, the current density was significantly reduced, indicating stabilization of the surface by the SEB initiator. This would be consistent with a smaller active surface area as a result of bonding of the initiator to the surface.

The polarization curve of the PMMA-covered copper electrode (curves c, d, and e) indicated that both the anodic and cathodic reactions were affected. Both arms moved to lower current density which was a reasonable expectation in the presence of a hydrophobic polymer layer, but the reduction in the anodic current was more notable than that of the cathodic current. This showed that the PMMA can reduce anodic dissolution and also retards the hydrogen evolution reaction. Otherwise, the anodic current decreased with the increase in the  $M_n$  of the PMMA and the shift in the corrosion potential ( $E_{\text{corr}}$ ) values to the noble direction was more significant as shown in Fig. 7.

## Electrochemical impedance spectroscopy

Measurements were performed to determine the impedance parameters of the naked copper/electrolyte, SEB monolayers-covered copper/electrolyte or PMMA-covered copper/electrolyte. Figure 8 was the Nyquist impedance spectroscopy for the naked copper and SEB self-assembled monolayers (SAMs) covered electrodes in 0.5 mol/L NaCl solution.

The Nyquist plot of naked copper measured in NaCl solution (see Fig. 8a) displayed an obvious capacitive loop deviating from an ideal semicircle in high frequency, which was bought by surface roughness and was known as the “dispersing effect”, and a straight line (Warburg impedance) in low frequency. The capacitive loop was attributed to the relaxation time constant of the charge-transfer resistance ( $R_{ct}$ ) whose value was approximately equal to the diameter of the capacitive loop and the double-layer capacitance ( $C_{dl}$ ) at the copper/electrolyte interface [31], and the Warburg impedance was due to diffusion of soluble reactant or product species [32]. Considering that the impedance of a double layer did not behave as an ideal capacitor in the presence of a dispersing effect, a constant phase element of double layer ( $CPE_{dl}$ ) was used as a substitute for the capacitor to fit more accurately the impedance behavior of the electric double layer. It had been calculated that the value of  $R_{ct}$  was  $810 \Omega \text{cm}^2$  using Zview impedance software. In the NaCl solution, the corrosion reaction at copper surface consisted of the anodic dissolution of copper and the cathodic reduction of the dissolved oxygen. Recent study showed that the diffusion process was controlled by diffusion of dissolved oxygen from the bulk solution to the electrode surface and the Warburg impedance was ascribed to diffusion of oxygen [33].

The impedance spectra of SEB monolayer covered copper electrodes were quite different from that of naked copper electrodes. In NaCl corrosive solution, the Warburg impedance observed previously in Fig. 8a disappeared, and only a depressed semicircle with diameter of more than  $5.67 \times 10^3 \Omega \text{cm}^2$  was observed.

Figure 9 was the Nyquist impedance spectra of copper electrode covered with different molecular weight of PMMA films in 0.5 mol/L NaCl solution. The

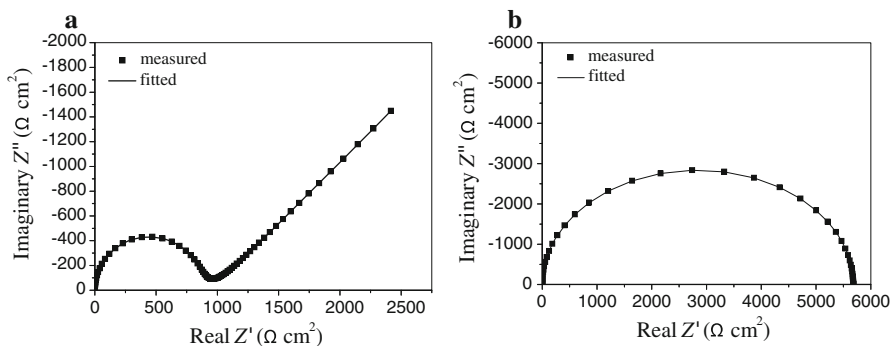


**Fig. 8** Nyquist impedance spectroscopy of **a** the naked copper electrode and **b** the SEB SAMs-covered copper electrode in 0.5 mol/L NaCl solution

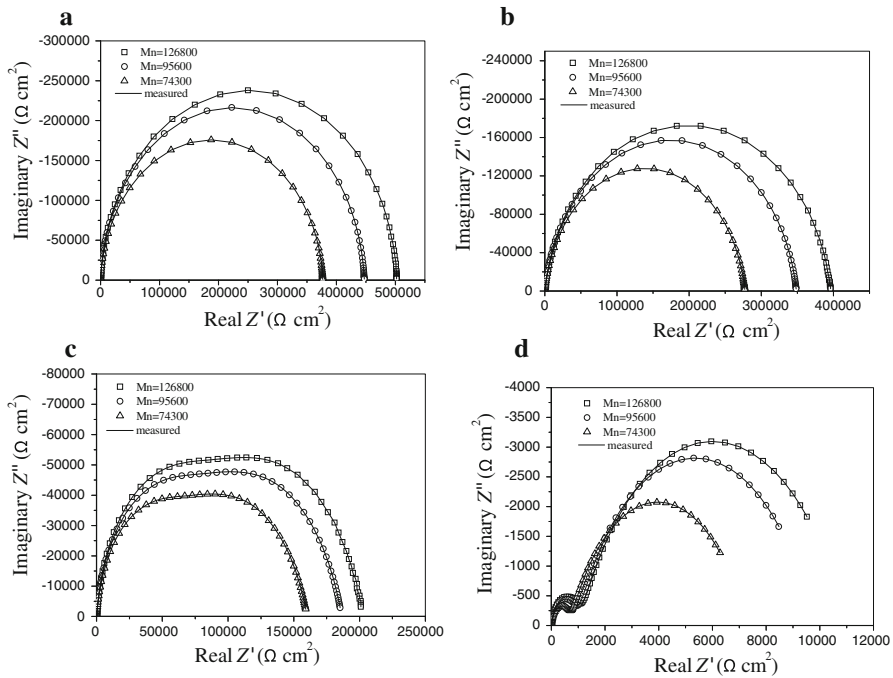


**Fig. 9** The variation of impedance spectroscopy for the PMMA-covered copper electrode with different molecular weight of PMMA under different immersion time in 0.5 mol/L NaCl solution: **a** 1 h, **b** 4 h, **c** 12 h, **d** 24 h

exposure time in NaCl solution and the molecular weight of PMMA were changed to investigate the inhibitive efficiency. The impedance spectra of PMMA-covered electrodes were different from that of the naked copper electrodes both in size and shape. Compared with the Nyquist spectroscopy of naked copper electrode, the diameter size of the semicircle of PMMA-covered copper electrode tended to be larger.

It was found from Fig. 9 that with the increasing of molecular weight of PMMA, the diameter size of the semicircle of PMMA-covered copper electrode tended to be larger, and with the exposure time extending, the diameter size of the semicircle became smaller. The larger diameters of the semicircle indicated the decreasing in corrosion rate of copper electrode under the protection of polymer layer. When time reached 24 h, the impedance spectra gave two poor-separated capacitive loops whose diameters were reduced with exposure time (Fig. 9d). The appearance of a low capacitive loop for long immersion times indicated occurrence of electrochemical corrosion reaction. It was meant that the polymer coating was damaged or degraded, and the aggressive ions and water penetrated though polymer coating and reacted with metal substrate, giving rise to the expansion of the defective sites and leading to further destruction of polymer coating.

Different equivalent circuits [34] have been established so far to interpret impedance behavior of the electrodes. However, these circuits are inconsistent with

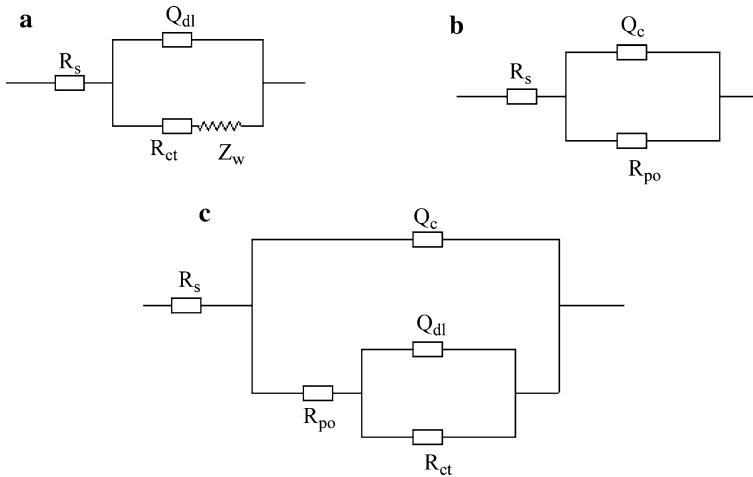


**Fig. 10** Equivalent circuits to fit the EIS for copper displaying **a** a Warburg impedance, **b** one capacitive loop, and **c** two capacitive loops

each other in interpreting the physical meaning of elements and explaining the origin of impedance loops. In this study, three ECs were proposed to model the respective impedance spectra of the naked and the surface-functionalized copper electrodes (Fig. 10). EC (a) is used to fit the impedance spectra of coupons with a compact surface film, EC (b) is used to model the impedance spectra of coupons with porous and non-protective surface film, while EC (c) has been widely used to estimate the barrier, protection and degradation of the polymer coatings.

In Fig. 10,  $R_s$  is the solution resistance between the working electrode and reference electrode;  $R_{ct}$  is the charge-transfer resistance corresponding to the corrosion reaction at metal substrate/solution interface;  $Q_{dl}$  is CPEs modeling the double-layer capacitance;  $Z_w$  the Warburg impedance attributes to mass transport in the process of corrosion reactions; the pore resistance ( $R_{po}$ ) represents the extent of ionic conduction through a polymer in an electrolytic environment, and is commonly used as a criterion for assessing the extent of corrosion protection derived from the organic coatings, while the CPEs of coating,  $Q_c$  is used to substitute coating capacitance,  $C_c$  by taking into account of the phenomena related to the heterogeneous surface and diffusion process.

The fitted parameters of the impedance spectra were summarized in Table 3. The quality of PMMA films can be evaluated by  $R_{po}$  and  $Q_c$  [35]. The more densely packed the layers, the larger the  $R_{po}$  values and the lower the  $C_c$  values. Value of  $n$  for the  $Q_c$  element can be used as an index to determine whether PMMA films behaved like a capacitor. The behavior of SAMs tended to be an ideal capacitor when value of  $n$  approaches +1 gradually.

From the data, it can be seen that the value of the charge-transfer resistance of the naked electrode was the lowest. When the surfaces of copper electrodes were covered with SEB films, the value of  $R_{ct}$  increased. In the case of the PMMA-covered copper,  $R_{po}$  values were significantly large, indicative of the decrease in

**Table 3** Fitting parameters of the EIS spectra for copper in 0.5 mol/L NaCl solution

|                      | Exposure time (h) | $R_s$ ( $\Omega$ cm <sup>2</sup> ) | $R_{ct}$ ( $\Omega$ cm <sup>2</sup> ) | $Q_{dl}$ (F/cm <sup>2</sup> ) | $Q_c$ (F/cm <sup>2</sup> )    |                       | $R_{po}$ ( $\Omega$ cm <sup>2</sup> ) | $Z_w$ ( $\Omega$ cm <sup>2</sup> ) |
|----------------------|-------------------|------------------------------------|---------------------------------------|-------------------------------|-------------------------------|-----------------------|---------------------------------------|------------------------------------|
|                      |                   |                                    |                                       |                               | $C_{dl}$ (F/cm <sup>2</sup> ) | $n$                   |                                       |                                    |
| Naked Cu             | –                 | 4.97                               | $0.81 \times 10^3$                    | $3.41 \times 10^{-6}$         | –                             | –                     | –                                     | $0.53 \times 10^{-3}$              |
| Monolayers on Cu     | –                 | 2.73                               | $5.67 \times 10^3$                    | $1.39 \times 10^{-6}$         | –                             | –                     | –                                     | –                                  |
| Cu–PMMA <sup>a</sup> | 1                 | 3.90                               | –                                     | –                             | –                             | $8.07 \times 10^{-7}$ | $5.03 \times 10^5$                    | 0.97                               |
| Cu–PMMA <sup>b</sup> | –                 | 4.86                               | –                                     | –                             | –                             | $8.71 \times 10^{-7}$ | $3.65 \times 10^5$                    | 0.96                               |
| Cu–PMMA <sup>c</sup> | –                 | 6.45                               | –                                     | –                             | –                             | $0.91 \times 10^{-6}$ | $2.56 \times 10^5$                    | 0.94                               |
| Cu–PMMA <sup>a</sup> | 4                 | 3.01                               | –                                     | –                             | –                             | $1.70 \times 10^{-6}$ | $4.00 \times 10^5$                    | 0.92                               |
| Cu–PMMA <sup>b</sup> | –                 | 1.22                               | –                                     | –                             | –                             | $3.96 \times 10^{-6}$ | $3.62 \times 10^5$                    | 0.91                               |
| Cu–PMMA <sup>c</sup> | –                 | 5.69                               | –                                     | –                             | –                             | $5.31 \times 10^{-6}$ | $2.41 \times 10^5$                    | 0.91                               |
| Cu–PMMA <sup>a</sup> | 12                | 7.06                               | $1.01 \times 10^5$                    | $1.22 \times 10^{-5}$         | –                             | $9.81 \times 10^{-6}$ | $1.02 \times 10^5$                    | 0.90                               |
| Cu–PMMA <sup>b</sup> | –                 | 4.79                               | $8.82 \times 10^3$                    | $7.69 \times 10^{-5}$         | –                             | $1.01 \times 10^{-5}$ | $8.43 \times 10^4$                    | 0.89                               |
| Cu–PMMA <sup>c</sup> | –                 | 4.88                               | $4.82 \times 10^3$                    | $4.58 \times 10^{-4}$         | –                             | $1.79 \times 10^{-5}$ | $4.82 \times 10^4$                    | 0.89                               |
| Cu–PMMA <sup>a</sup> | 24                | 3.24                               | $9.82 \times 10^3$                    | $1.15 \times 10^{-3}$         | –                             | $2.35 \times 10^{-5}$ | $1.13 \times 10^3$                    | 0.88                               |
| Cu–PMMA <sup>b</sup> | –                 | 3.32                               | $5.13 \times 10^3$                    | $1.83 \times 10^{-3}$         | –                             | $3.33 \times 10^{-5}$ | $0.87 \times 10^3$                    | 0.86                               |
| Cu–PMMA <sup>c</sup> | –                 | 2.09                               | $3.58 \times 10^3$                    | $2.47 \times 10^{-3}$         | –                             | $4.64 \times 10^{-5}$ | $0.56 \times 10^3$                    | 0.85                               |

<sup>a</sup> The  $M_n$  of PMMA is  $1.27 \times 10^5$ ,  $M_w/M_n$  is 1.37. The polymerization time is 11 h

<sup>b</sup> The  $M_n$  of PMMA is  $9.56 \times 10^4$ ,  $M_w/M_n$  is 1.40. The polymerization time is 6 h

<sup>c</sup> The  $M_n$  of PMMA is  $7.43 \times 10^4$ ,  $M_w/M_n$  is 1.59. The polymerization time is 2 h

corrosion rate under the protection of polymer layer. On the other hand,  $R_{po}$  and  $R_{ct}$  values increase with the enhancement of  $M_n$  of PMMA films, indicative of the substantial increase in barrier property of the polymer coating against the penetration of aggressive ions and water. However, it can be seen that, the longer the immersion time was, the smaller value of  $R_{po}$  and  $n$  was. This indicated that the behavior of PMMA films was deviating gradually from a pure capacitor with extending the immersion time. The capacitance ( $Q_c$ ) of coating as a function of exposure time in an electrolyte solution provided information on stability of the coating and the extent of water uptake.  $Q_c$  increased gradually with exposure time, indicative of the uptake of the electrolyte and water by the polymer coatings, and thus the decrease in protective capability of the polymer coating.

## Conclusion

A new initiator SEB was synthesized and utilized in ATRP of MMA with CuBr/2,2'-bpy as the catalyst and DMF as the solvent. With this new initiating system, the number-average molecular weights of polymers increase with increasing monomer conversion and the kinetics are first order in monomer.  $M_w/M_n$  of PMMA was as low as 1.34, but the initiator efficiency is not high. The obtained well-defined PMMA functionalized with salicylidene-1,2-ethanediaminoethyl and  $\omega$ -Br as the end groups were characterized by FT-IR spectroscopy and used as macroinitiators for chain-extension reaction. Then, PMMA coatings were grafted from copper substrates by SI-ATRP from a surface-bound SEB initiator. The EIS measurements and potentiodynamic electrochemical experiments confirmed the successful grafting of the polymer coatings. Greatly improved short-term anticorrosive properties for PMMA modified electrodes were demonstrated by substantially increased resistance for a period of 24 h as compared to bare copper.

**Acknowledgment** We gratefully acknowledge the support of this work by the Analysis Center of China Pharmaceutical University.

## References

1. Matyjaszewski K, Xia J (2001) Atom transfer radical polymerization. *Chem Rev* 101:2921–2990
2. Percec V, Barboiu B (1995) 'Living' radical polymerization of styrene initiated by arenesulfonyl chlorides and  $Cu^I(bpy)_nCl$ . *Macromolecules* 28:7970–7971
3. Wang JS, Matyjaszewski K (1995) 'Living'/controlled radical polymerization. Transition-metal-catalyzed atom transfer radical polymerization in the presence of a conventional radical initiator. *Macromolecules* 28:7572–7573
4. Teodorescu M, Matyjaszewski K (2000) Controlled polymerization of (meth)acrylamides by atom transfer radical polymerization. *Macromol Rapid Commun* 21:190–194
5. Wang G, Zhu XL, Cheng ZP, Zhu J (2005) Atom transfer radical polymerization of styrene initiated by the novel initiator 2-bromo-2-nitropropane. *E-polymers* no. 035
6. Tang W, Matyjaszewski K (2007) Effects of initiator structure on activation rate constants in ATRP. *Macromolecules* 40:1858–1863
7. Wang G, Zhu XL, Cheng ZP, Zhu J (2003) Reverse atom transfer radical polymerization of methyl methacrylate with  $FeCl_3$ /pyromellitic acid. *Eur Polym J* 39:2161–2165



8. Zhu C, Sun F, Zhang M, Jin J (2004) Atom transfer radical suspension polymerization of methyl methacrylate catalyzed by CuCl/bpy. *Polymer* 45:1141–1146
9. Nanda AK, Matyjaszewski K (2003) Effect of [PMDETA]/[Cu(I)] ratio, monomer, solvent, counterion, ligand, and alkyl bromide on the activation rate constants in atom transfer radical polymerization. *Macromolecules* 36:1487–1493
10. Kato M, Kamigaito M, Sawamoto M, Higashimura T (1995) Polymerization of methyl methacrylate with the carbon tetrachloride/dichlorotris-(triphenylphosphine)ruthenium(II)/methylaluminum bis(2, 6-di-tert-butylphenoxide) initiating system: possibility of living radical polymerization. *Macromolecules* 28:1721–1723
11. Kamigaito M, Ando T, Sawamoto M (2001) Metal-catalyzed living radical polymerization. *Chem Rev* 101:3689–3745
12. Arslan A, Kralp S, Toppare L, Bozkurt A (2006) Novel conducting polymer electrolyte biosensor based on poly(1-vinyl imidazole) and poly(acrylic acid) networks. *Langmuir* 22:2912–2915
13. Zhu AH, Wang Z, Xie MR, Zhang YQ (2007) Synthesis of imidazole end-capped poly(*n*-butyl methacrylate)s via atom transfer radical polymerization with a new functional initiator containing imidazolium group. *E-polymers* no. 009
14. He XY, Yang W, Pei XW (2008) Preparation, characterization, and tunable wettability of poly(ionic liquid) brushes via surface-initiated atom transfer radical polymerization. *Macromolecules* 41:4615–4621
15. Rannard SP, Davis NJ, Herbert I (2004) Synthesis of water soluble hyperbranched polyurethanes using selective activation of AB(2) monomers. *Macromolecules* 37:9418–9430
16. Matyjaszewski K, Wang JL, Grimaud T, Shipp DA (1998) Controlled/‘living’ atom transfer radical polymerization of methyl methacrylate using various initiation systems. *Macromolecules* 31:1527–1534
17. Coessens V, Pintauer T, Matyjaszewski K (2001) Functional polymers by atom transfer radical polymerization. *Prog Polym Sci* 26:337–377
18. Roy D, Semsarilar M, Guthire JT, Perrier S (2009) Cellulose modification by polymer grafting: a review. *Chem Soc Rev* 38:2046–2064
19. Nguyen S, Marchessault RH (2005) Atom transfer radical copolymerization of bacterial poly(3-hydroxybutyrate) macromonomers and methyl methacrylate. *Macromolecules* 38:290–296
20. Advincula RC, Brittain WJ, Caster KC (2005) *Polymer Brushes*. Wiley, New York
21. Prucker O, Ruhe J (1998) Mechanism of radical chain polymerizations initiated by azo compounds covalently bound to the surface of spherical particles. *Macromolecules* 31:602–613
22. Prucker O, Ruhe J (1998) Synthesis of poly(styrene) monolayers attached to high surface area silica gels through self-assembled monolayers of azo initiators. *Macromolecules* 31:592–601
23. Fan XW, Li LJ, Dalsin JL, Messersmith PB (2005) Biomimetic anchor for surface-initiated polymerization from metal substrates. *J Am Chem Soc* 127:15843–15847
24. Feng W, Brash JL, Zhu SP (2005) Adsorption of fibrinogen and lysozyme on silicon grafted with poly(2-methacryloyloxyethyl phosphorylcholine) via surface-initiated atom transfer radical polymerization. *Langmuir* 21:5980–5987
25. Granville AM, Brittain WJ (2004) Stimuli-responsive semi-fluorinated polymer brushes on porous silica substrates. *Macromol Rapid Commun* 25:1298–1302
26. Patten TE, Xia J, Abernathy T, Matyjaszewski K (1996) Polymers with very low polydispersities from atom transfer radical polymerization. *Science* 272:866–868
27. Jordan R, Ulman A (1999) Surface-initiated anionic polymerization of styrene by means of self-assembled monolayers. *J Am Chem Soc* 121:1016–1022
28. Zhao B, Brittain WJ (2000) Polymer brushes: surface-immobilized macromolecules. *Prog Polym Sci* 25:677–710
29. Chen RX, Zhu SP, Maclaughlin S (2008) Grafting acrylic polymers from flat nickel and copper surfaces by surface-initiated atom transfer radical polymerization. *Langmuir* 24:6889–6896
30. Brown HC, Berneis HL (1953) Steric strains as a factor in the solvolytic reactions of neopentyl-dimethyl and dioneopentylmethylcarbinyl chlorides. *J Am Chem Soc* 75:10–14
31. Barcia OE, Matoos OR (1990) Reaction model simulating the role of sulphate and chloride in anodic dissolution of iron. *Electrochim Acta* 35:1601–1608
32. Ma H, Chen S, Niu L, Shang S, Zhao S, Li S, Quan ZJ (2001) Studies on electrochemical behavior of copper in aerated NaBr solutions with schiff base, N,N#-o-phenylen-bis(3-methoxysalicylideneimine). *J Electrochem Soc* 148:B208–B216

33. Ma H, Chen S, Niu L, Zhao S, Li S, Li D (2002) Inhibition of copper corrosion by several Schiff bases in aerated halide solutions. *J Appl Electrochem* 32:65–72
34. Zamborini FP, Crooks RM (1998) Corrosion passivation of gold by n-alkanethiol self-assembled monolayers: effect of chain length and end group. *Langmuir* 14:3279–3286
35. Feng Y, Teo WK, Siow KS, Gao Z, Tan KL, Hsieh AK (1997) Corrosion protection of copper by a self-assembled monolayer of alkanethiol. *J Electrochem Soc* 144:55–64